# Identification of High Affinity Fatty Acid Binding Sites on Human Serum Albumin by MM-PBSA Method

Shin-ichi Fujiwara and Takashi Amisaki
Department of Biological Regulation, Faculty of Medicine, Tottori University, Yonago, Japan

ABSTRACT Human serum albumin (HSA) has seven common fatty acid (FA) binding sites. In this study, we used the molecular mechanics Poisson-Boltzmann surface area method to identify high affinity FA binding sites on HSA in terms of binding free energy. Using multiple HSA-FA (myristate, palmitate) complex models constructed by molecular dynamics simulations, two methods were performed in molecular mechanics Poisson-Boltzmann surface area, the "three-trajectory method" and the "single-trajectory method". The former, which is less precise than the latter but may be more accurate as it includes the effects of conformational change upon binding, was used to classify high and low affinity sites. As a result, Sites 2, 4, and 5 were identified as high affinity sites for both FAs. The latter method, which is precise because energies are calculated from snapshots of the same trajectory for HSA-FA complex, was performed to compare the magnitude of binding free energy for these sites. The order of magnitude was $5 > 4 > 2$, identical to that of a previous publication by others. In this way, a combination of the two methods was effectively used to identify high affinity sites. This study therefore provides an insight into the quantitative identification of high affinity FA binding sites on HSA.

## INTRODUCTION

Human serum albumin (HSA) is a major protein component of blood plasma. It serves as a transport protein for several endogenous compounds, such as unesterified fatty acids (FA) and bilirubin, and is also capable of binding a broad spectrum of therapeutic agents. Drug binding to HSA can result in a prolonged in vivo half-life. Thus, the binding property of drugs to HSA is one of the most important factors determining their pharmacokinetics (1).

HSA consists of 585 amino acids and has a molecular mass of 66,500 Da. Recently, three-dimensional structures of HSA have been obtained by x-ray crystallography (2–4). The structure of HSA consists of three homologous domains (domains I–III), each of which is divided into two subdomains, A and B, having six and four $\alpha$-helices, respectively. For these subdomains, the positions and architecture of a broad spectrum of drugs have been identified by x-ray crystallography of HSA-drug complexes (5). The positions and architecture of FA binding sites on HSA have been also identified for these subdomains (6–9). Seven common FA binding sites have been identified for medium and long-chain FAs (8), and monosaturated and polyunsaturated FAs (9).

Under normal physiological conditions, HSA binds with ~0.1–2 mol of FA, per mol of protein (10). However, the molar ratio of FA/HSA can rise up to 6 during fasting or maximum exercise, resulting from an increase in FA in blood plasma (11,12). Drug binding to HSA can be modulated by simultaneous binding of FAs (1,5,13), therefore it is important to clarify the binding affinity of FA at each FA binding site on HSA. Very recently, the locations of high affinity FA binding sites on HSA have been reported (14–16). Simard et al. showed three high and four low affinity FA binding sites of palmitate (PLM) on HSA by combining $^{13}C$ NMR spectroscopy with drug-competition analysis (15). Kragh-Hansen et al. investigated high affinity binding sites of octanoate, decanoate, laurate, and myristate (MYR) by site-directed mutagenesis of HSA (16). Although these works give an insight into the binding of FA to HSA, they do not compare the absolute binding affinity of each FA binding site.

Several theoretical methods have recently been developed to estimate the binding free energy between protein and ligand, such as free energy perturbation (FEP) (17), the linear interaction energy (LIE) method (18), and the molecular mechanics Poisson-Boltzmann surface area (MM-PBSA) method (19). Of these methods, MM-PBSA is promising because it requires less computer resources than FEP and, contrary to LIE, applies no empirical parameters in its free energy calculations. In MM-PBSA, the binding free energy of a given protein-ligand complex is calculated by summing up molecular mechanical energies, solvation energies, and entropic terms. In addition, by performing molecular dynamics (MD) simulation of the given protein-ligand complex, the ensemble averages of these properties are obtained. MM-PBSA method has been successfully applied to several ''multiple ligands bound to one binding site'' systems (20–25). As far as we know, however, there are no published works that apply the MM-PBSA method to a ''one ligand bound to multiple binding sites'' system.

This study was undertaken to quantitatively elucidate high and low affinity FA binding sites on HSA by MM-PBSA calculations. This is the first report that has applied MM-PBSA to a ''one ligand (FA) bound to multiple binding sites (on HSA)'' system. We focused on the binding of PLM, one

*Submitted April 25, 2007, and accepted for publication August 31, 2007.*

Address reprint requests to Shin-ichi Fujiwara, PhD, Dept. of Biological Regulation, Faculty of Medicine, Tottori University, Yonago, Tottori 683-8503, Japan. Tel.: 81-859-38-6358; Fax: 81-859-38-6350; E-mail: fujiwara@grape.med.tottori-u.ac.jp.

Editor: Ron Elber.

© 2008 by the Biophysical Society
0006-3495/08/01/95/09 $2.00

doi: 10.1529/biophysj.107.111377

of the most common FAs transported by HSA in plasma (26), and MYR, commonly used for examining the effect of FA on HSA (5,13). In this article, we present the calculated binding free energy results of two methods, termed the ''three-trajectory method'' and the ''single-trajectory method''. The former is used to classify high and low affinity FA binding sites, and the latter to compare the magnitude of binding free energy among high affinity sites identified by the former. Based on the MM-PBSA results, we compare the calculated binding free energy with the experimental multiple binding constants (27–29). In addition, we show that conformational changes in HSA by the binding of one FA molecule differed according to the binding site.

## MATERIALS AND METHODS

### Starting structure of HSA-FA complex

The initial coordinates of HSA-FA complex were obtained from the Protein Data Bank (PDB) (30) (HSA-PLM complex, 1E7H; HSA-MYR complex, 1E7G; the resolutions of the structures were 2.4 and 2.5 Å, respectively). In PDB entry 1E7H (8), seven PLM molecules were bound to HSA, and all were included in the following MD simulations (HSA-7PLM complex). On the other hand, eight MYR molecules were bound to HSA in PDB entry 1E7G (8). In this study, MYR bound to Site 2′ was removed because seven molecules were bound to the sites, in common with all medium- and long-chain FAs (8,9). Hence, seven MYR molecules were included in the following MD simulations (HSA-7MYR complex; Fig. 1).

### Molecular dynamics simulations of HSA-FA complex

A series of MD calculations were carried out using the AMBER8 package (31). The LEaP module was used for model construction of HSA-FA complex. The sander module was used for energy minimization, and the ''pmemd'' module was used for MD calculations. The AMBER (parm94) force field (32) was used for modeling the HSA system. PLM and MYR force fields were generated by the antechamber module, based on the general AMBER force field (GAFF) (33). Following ab initio optimization of FA molecule at the HF/6-31G* level by Gaussian 03 (34), a restrained electrostatic potential fit procedure (35) was used as the charge method in GAFF. Missing residues in the starting structure of HSA (residues 1, 2, 584, 585) were added by the Build and Edit Protein tool on DISCOVERY STUDIO (version 1.5) (36). Following the addition of missing residues, missing atoms were added by the LEaP module. Energy minimization with constraints on the positions of heavy atoms was carried out for 500 steps. $Na^+$ counterions were placed by LEaP to neutralize the negative charges of both HSA-FA complex models at pH 7. A rectangular-shaped box of water was constructed using the TIP3P water model (37), with the buffering distance set to 12 Å. The resulting model systems contained 97,447 (HSA-7PLM complex) and 98,473 (HSA-7MYR complex) atoms. The single FA molecule system was also constructed according to the same criterion, and the model systems contained 3662 (PLM molecule) and 3440 (MYR molecule) atoms. For each system, 500 steps of energy minimization constraining the HSA and/or FA molecules were carried out, followed by 500 steps of energy minimization with no constraints. After energy minimization, 8-ns MD calculations were carried out for each HSA-seven FA complex model (HSA-7FA) under periodic boundary conditions. The nonbonded list was generated using an atom-based cutoff of 8 Å. The long-range electrostatic interactions were handled by the particle-mesh Ewald algorithm (38). The time step of the MD simulations was set to 2.0 fs, and the SHAKE algorithm (39) was used to constrain bond lengths at their equilibrium values. Temperature and pressure were maintained using the weak-coupling algorithm (40) with coupling constants $\tau_T$ and $\tau_P$ of 1.0 and 0.2 ps, respectively (310 K, 1 atm). Coordinates were saved for analyses every 1 ps.

Seven HSA-one FA complex models (HSA-1FAs) and the unliganded HSA model were obtained by removing six or seven other FA molecules from the snapshot of HSA-7FA complex at 4 ns, with the velocity of each atom unchanged from that at 4 ns, to prevent from sampling different conformational space between the HSA models. Starting with seven HSA-1FA complex models and one unliganded HSA model, additional 4-ns MD simulations were performed for each model under the same conditions as above.

The MD simulations and subsequent MM-PBSA calculations were run on an in-house PC cluster composed of eight nodes (AMD Opteron 2.2 GHz, 2 GB DDR memory; Sunnyvale, CA) with a gigabit Ethernet interconnection.

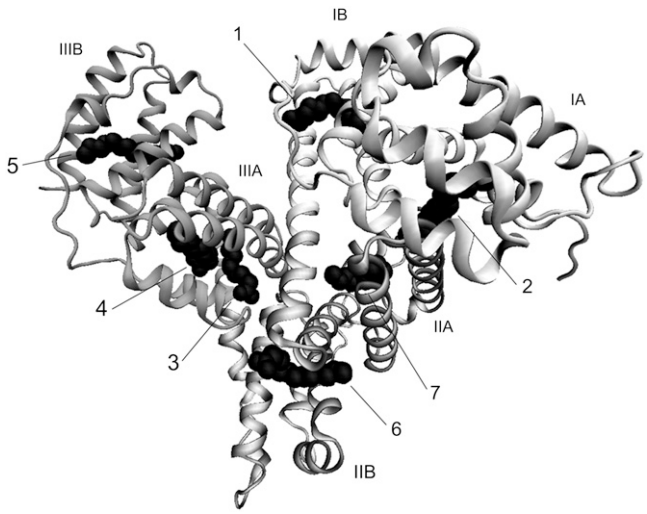


FIGURE 1 Ribbon model of HSA-MYR complex, derived from x-ray crystallography (PDB entry 1E7G). HSA is composed of three homologous domains I–III, each of which is divided into two subdomains, A and B. The seven MYR molecules are shown in black in a space-filling representation. Numbering of the sites is taken from Bhattacharya et al. (8). This diagram was generated using visual molecular dynamics (VMD version 1.8.5) (51).

### MM-PBSA calculations for binding free energy

Binding free energy ($\Delta G_{bind}$) of FA at each FA binding site on HSA was calculated as follows:

$$\Delta G_{bind} = G^{complex} - G^{HSA} - G^{FA}, \quad (1)$$

where $G^{complex}$, $G^{HSA}$, and $G^{FA}$ are the free energies of complex, HSA, and FA, respectively. Free energy ($G$) of each state was calculated as follows:

$$G = E_{MM} + G_{PB} + G_{SA} - TS \quad (2)$$

$$E_{MM} = E_{vdw} + E_{ele} + E_{int}, \quad (3)$$

where $E_{MM}$ is the molecular mechanical energy, $G_{PB}$ and $G_{SA}$ are the contributions from polar and nonpolar terms of the free energy of the solvent continuum, and $TS$ is the entropic contribution of the solute. $E_{MM}$ was obtained by summing contributions from internal energies including bond, angle, and torsional angle energies ($E_{int}$), electrostatic energy ($E_{ele}$), and van der Waals energy ($E_{vdw}$), using the same force field as that of MD simulations with no cutoff. $G_{PB}$ was calculated using the DELPHI program (41) with PARSE (42) atom radii and standard AMBER94 charges (32) for amino acids. The dielectric constants inside and outside the molecule were

1.0 and 80.0, respectively. $G_{SA}$ was calculated using a solvent accessible surface area (*SASA*) as follows:

$$G_{SA} = \gamma \times SASA + b. \quad (4)$$

The *SASA* was computed with the ''molsurf'' module in AMBER8 (31), using a probe radius of 1.4 Å. The surface tension proportionality constant ($\gamma$) and the free energy of nonpolar solvation for a point solute ($b$) were set to 0.00542 kcal/mol/Å$^2$ and 0.92 kcal/mol, respectively (42). Estimates of conformational entropies were computed with the ''nmode'' module in AMBER8 (30). Entropic contributions from translational and rotational motion were taken from classical statistical thermodynamics (43), and entropic contribution from vibrational motion was obtained by normal mode analysis (44). Following energy minimization of the snapshot with a distance-dependent dielectric function ($\varepsilon = 4R_{ij}$) until the root mean-square of the elements of the gradient vector was $<10^{-4}$ kcal/mol/Å, frequencies of the vibrational modes were computed at 300 K for the minimized structures using a harmonic approximation of the energies.

For the binding free energy calculations by MM-PBSA, 500 snapshots of each model were taken at time intervals of 6 ps from the 3-ns production runs (5–8 ns). However, entropic contributions were evaluated for only 20 snapshots taken at time intervals of 150 ps from the 3-ns production runs, because of the rather large computational expense. In addition, only subdomains of HSA that participated in the binding of FA were used for calculating the entropic contribution (Site 1, IB; Site 2, IA, IB, IIA; Site 3, IIB, IIIA; Site 4, IIIA; Site 5, IIIB; Site 6, IIA, IIB; Site 7, IB, IIA).

### Three-trajectory method and single-trajectory method

In these MM-PBSA calculations, two trajectory set methods were performed. The ''three-trajectory method'' used snapshots extracted from three trajectories of complex, FA, and unliganded HSA and the ''single-trajectory method'' used snapshots extracted from a single trajectory of the HSA-FA complex. The binding free energy of the three-trajectory method was calculated as follows:

$$\Delta G_{bind} = \langle G^{complex} \rangle - \langle G^{HSA} \rangle - \langle G^{FA} \rangle, \quad (5)$$

where $\langle \cdots \rangle$ denotes an average of snapshots taken from MD trajectories. The binding free energy was calculated for the single-trajectory method, as follows:

$$\Delta G_{bind} = \langle G^{complex} - G^{HSA} - G^{FA} \rangle. \quad (6)$$

It should be noted that the change in internal energies ($\Delta E_{int}$) equals zero in calculating the binding free energy according to Eq. 6, since the internal energies of the complex and the separated parts are calculated from the same trajectory.

## RESULTS AND DISCUSSION

### Root mean-square deviation of HSA-FA complex and unliganded HSA

The root mean-square deviation (RMSD) of $C_\alpha$ atoms from the x-ray structure in HSA-FA complex systems are shown in Fig. 2. In each system, RMSD values reached plateau at ~2 ns (see Fig. 2 *A*). Calculated from the 4- to 8-ns trajectory data, the RMSD values of $C_\alpha$ atoms in the whole HSA molecules were 2.58 ± 0.23 Å and 3.03 ± 0.23 Å for HSA-7MYR complex and HSA-7PLM complex, respectively. We also calculated the RMSD of $C_\alpha$ atoms in each subdomain to analyze which region of HSA undergoes large conformational changes (Fig. 3). In both HSA-7FA models, subdomains IA and IIIB showed larger RMSD values, suggesting that larger conformational changes occur at these subdomains. Some of the recent MD studies, which were carried out under similar conditions with these MD simulations, reported that the RMSD values reached between 2 and 4 Å (45,46). Taking into account of the relatively low resolution of the crystal structures of HSA (2.4–2.5 Å), we conclude that no significant structural drift from the x-ray structure occurred during the MD simulations.

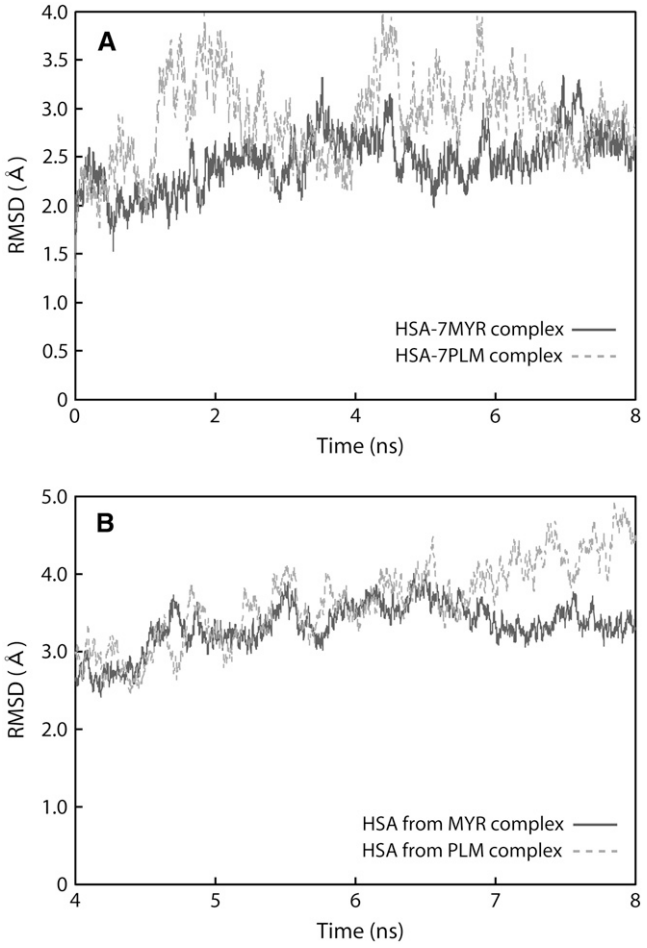


FIGURE 2 Time evolution of the RMSD of $C_\alpha$ atoms from the starting structure during 8-ns MD simulations of HSA-7FA complex models (*A*), and 4- to 8-ns simulations of unliganded HSA models (*B*).

Additional 4-ns MD of unliganded HSA models also showed that no significant structural drift occurred during the MD simulations and that RMSD values reached plateau at ~5 ns in both systems (Fig. 2 *B*). For the HSA-1FA complex models, RMSD also reached plateau at ~5 ns (see Supplementary Material). In comparisons of the unliganded HSA models with the crystal structure of unliganded HSA (PDB entry 1AO6), RMSD values of $C_\alpha$ atoms in the whole HSA molecule were 3.40 ± 0.20 Å (from HSA-7PLM complex) and 5.07 ± 0.40 Å (from HSA-7MYR complex), calculated from the 5- to 8-ns trajectory. Although the RMSD value

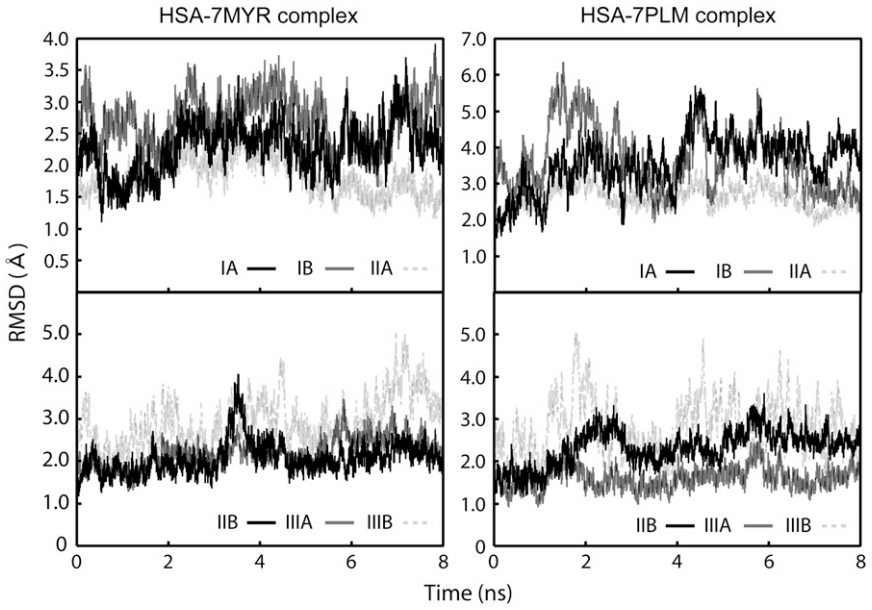


FIGURE 3 Time evolution of the RMSD of $C_\alpha$ atoms belonging to each subdomain of HSA-7FA complex model from the starting structure during 8-ns MD simulations. All $C_\alpha$ atoms were fitted to the starting structure.

from the crystal structure was large in unliganded HSA model constructed from the HSA-7MYR complex, the RMSD value in each FA binding site (Site 1–7) was between 2 and 4 Å, suggesting that no significant structural drift from the crystal structure occurred in each FA binding site on HSA. Therefore, the deviations from the crystal structure observed as above may not affect significantly the binding free energy calculation by the three-trajectory method. In this study, we used from 5- to 8-ns trajectories in the following MM-PBSA calculations.

## Two types of MM-PBSA for identifying high affinity FA sites

The single-trajectory method (Eq. 6) has been used in many MM-PBSA studies owing to the considerable reduction in computer time due to MD simulation for only one complex model (20,21,25,47). On the basis that large conformational changes do not occur upon binding, the single-trajectory approach has the benefit of error cancellation in internal energies ($\Delta E_{\text{int}}$) and high correlation between variations of $G^{\text{complex}}$ and ($G^{\text{HSA}} + G^{\text{FA}}$), resulting in precise estimation of the binding free energy. In this study, however, conformational changes of HSA by the binding of FAs have been reported (6,48), and the contribution of each FA binding site to the conformational changes upon FA binding may be different. Therefore, the single-trajectory method, which cannot include the effect of conformational changes on HSA by the binding of FA, may not be appropriate for ranking the binding free energies among FA binding sites with conformational changes.

On the other hand, the three-trajectory method (Eq. 5) does have value in that it may calculate total free energy change, including intramolecular strain, characterized as $\Delta E_{\text{int}}$, and an induced fit effect, by the binding of FA on HSA. In fact, some articles reported the significant effect of including $\Delta E_{\text{int}}$ in the binding free energy (47,49). However, the three-trajectory method is less precise compared to the single-trajectory method because it includes an additional source for errors, the contribution of internal energy term ($\Delta E_{\text{int}}$), and does not include cancellation of errors derived from correlation between variations of $G^{\text{complex}}$ and ($G^{\text{HSA}} + G^{\text{FA}}$) (23,47). Because of the additional errors, the three-trajectory method may not be appropriate for ranking the binding free energy of each FA binding site, especially with similar binding conformations.

In this study, based on the characteristics of the two types of MM-PBSA as mentioned above, we used the two methods in the following way: in comparisons between FA binding sites where large conformational changes can occur upon binding, the three-trajectory method may be more accurate for calculation of binding free energy than the single-trajectory method. Furthermore, contributions from each energy component in HSA-FA interactions are assumed to be quite different between high affinity and low affinity sites. Taking these points into account, we first used the three-trajectory method to classify high and low affinity FA binding sites on HSA. In addition, even if conformational changes occur upon FA binding, it can be expected that, at favorable FA binding sites, a given FA molecule binds to each site in a similar way. Thus the binding energies can be compared between the sites, although some bias, which is in common with all the sites, may be involved in the estimation. Based on this assumption, we next used the single-trajectory method to compare the magnitude of binding free energy between high FA binding sites.

## MM-PBSA for binding of palmitate on HSA

Table 1 shows the calculated binding free energy components of HSA-1PLM complex based on the three-trajectory method. The binding free energy ($\Delta G_{bind}$) indicated large positive values at Sites 6 and 7. In the first published work regarding x-ray crystallographic analysis of HSA-MYR complex, only Sites 1–5 were detected using a lower FA to protein molar ratio (6), suggesting that Sites 6 and 7 are low affinity FA binding sites. The results of this study were consistent with those of previous work. In addition, the binding free energy indicated large positive values at Site 3 (18.0 kcal/mol), which is also in accordance with previous work reporting that the binding of PLM at Site 3 is weak (15). Consequently, we identified Sites 3, 6, and 7 as low affinity PLM binding sites. Simard et al. (15) reported that three high (Sites 2, 4, and 5) and four low PLM binding sites (Sites 1, 3, 6, and 7) exist on HSA. In this study, the magnitude of the binding free energy at Site 1 (although a negative value was indicated) was much smaller than that of Sites 2, 4, and 5 (Table 1), suggesting that the binding affinity at Site 1 is weaker than that of the other three sites.

Table 2 shows the calculated binding free energy components of HSA-1PLM complex using the single-trajectory method. Focused on high affinity binding sites identified by the three-trajectory method (Sites 2, 4, and 5), the order of the binding free energy was $5 > 4 > 2$. This result was in line with previous work by Simard et al. (15). Because the other PLM binding sites (Sites 1, 3, 6, 7) were already identified as low affinity sites by the three-trajectory method, we did not include these binding sites in comparison of the binding free energy by the single-trajectory method, although the binding free energy at Sites 1 and 3 indicated relatively large negative values by the single-trajectory method. If only the result of single-trajectory method was used, the trend of binding affinity was $5 > 1 > 3 > 4 > 2 > 7 > 6$, and Sites 1 and 3 might be misclassified as high affinity FA binding sites.

In summary, we identified Sites 2, 4, and 5 as high affinity PLM binding sites, where Site 5 was the highest affinity binding site. In addition, this study indicated that a combination of the three-trajectory and single-trajectory methods are effective in MM-PBSA calculations for determining high and low affinity binding sites, and the order of affinity for the high affinity sites.

**TABLE 1 Binding free energy components of HSA-1PLM complex in the three-trajectory method (in units of kcal/mol)**

| | $\Delta E^{*}_{ele}$ | $\Delta E_{vdw}$ | $\Delta E_{int}$ | $\Delta G_{SA}$ | $\Delta G_{PB}$ | $\Delta G^{\dagger}_{mmpbsa}$ | $T\Delta S^{\ddagger}$ | $\Delta G^{\S}_{bind}$ |
|---|---|---|---|---|---|---|---|---|
| Site 1 | 166.7 | −19.1 | −2.9 | −1.8 | −175.8 | −32.9 | −20.5 | −12.4 |
| | (9.8) | (2.4) | (4.4) | (0.1) | (9.1) | (5.7) | (1.5) | (5.9) |
| Site 2 | 131.1 | 12.0 | −2.3 | −2.6 | −262.2 | −124.0 | −15.8 | −108.1 |
| | (10.7) | (2.6) | (4.4) | (0.2) | (10.7) | (5.5) | (3.3) | (6.4) |
| Site 3 | 65.0 | −24.2 | 4.6 | −4.9 | −43.2 | −2.8 | −20.8 | 18.0 |
| | (9.9) | (2.4) | (4.4) | (0.1) | (10.7) | (5.6) | (2.5) | (6.2) |
| Site 4 | 111.1 | −21.3 | 0.9 | −3.0 | −151.4 | −63.7 | −17.9 | −45.8 |
| | (9.6) | (2.5) | (4.4) | (0.1) | (9.7) | (5.7) | (1.9) | (6.0) |
| Site 5 | 16.5 | 0.7 | −25.2 | −0.7 | −40.3 | −49.0 | −16.2 | −32.8 |
| | (8.7) | (2.5) | (4.4) | (0.1) | (8.7) | (5.3) | (1.6) | (5.5) |
| Site 6 | 87.6 | −14.5 | −5.9 | −3.6 | −44.7 | 18.8 | −23.7 | 42.4 |
| | (9.4) | (2.5) | (4.4) | (0.1) | (9.4) | (5.6) | (2.5) | (6.2) |
| Site 7 | 187.3 | −44.1 | −2.5 | −6.1 | −120.3 | 14.3 | −19.6 | 33.8 |
| | (8.6) | (2.4) | (4.2) | (0.1) | (8.8) | (5.2) | (2.8) | (5.9) |

*Number in parentheses is mean ± SE.

†$\Delta G_{mmpbsa} = \Delta G_{ele} + \Delta G_{vdw} + \Delta G_{int} + \Delta G_{SA} + \Delta G_{PB}$.

‡The absolute temperature ($T$) was set to 300 K in the MM-PBSA calculations.

§$\Delta G_{bind}$ was calculated according to Eq. 5.

**TABLE 2 Binding free energy components of HSA-1PLM complex in the single-trajectory method (in units of kcal/mol)**

| | $\Delta E_{ele}$ | $\Delta E_{vdw}$ | $\Delta G_{SA}$ | $\Delta G_{PB}$ | $\Delta G_{mmpbsa}$ | $T\Delta S$ | $\Delta G_{bind}$ |
|---|---|---|---|---|---|---|---|
| Site 1* | −10.5 | −43.8 | −5.7 | 27.9 | −32.1 | −21.0 | −11.0 |
| | (0.2) | (0.1) | (0.007) | (0.2) | (0.2) | (0.9) | (0.9) |
| Site 2 | −4.4 | −41.5 | −6.0 | 23.7 | −28.1 | −20.0 | −8.1 |
| | (0.2) | (0.1) | (0.008) | (0.3) | (0.2) | (2.1) | (2.2) |
| Site 3 | −12.9 | −44.5 | −5.5 | 34.1 | −28.8 | −19.6 | −9.2 |
| | (0.1) | (0.1) | (0.008) | (0.2) | (0.2) | (1.4) | (1.4) |
| Site 4 | −13.2 | −45.7 | −5.8 | 35.7 | −28.9 | −20.0 | −8.9 |
| | (0.2) | (0.1) | (0.004) | (0.2) | (0.2) | (1.5) | (1.5) |
| Site 5 | −23.2 | −46.4 | −5.6 | 45.0 | −30.2 | −18.1 | −12.0 |
| | (0.4) | (0.1) | (0.006) | (0.3) | (0.2) | (1.1) | (1.1) |
| Site 6 | −6.4 | −44.8 | −5.6 | 29.8 | −27.0 | −23.4 | −3.6 |
| | (0.2) | (0.1) | (0.005) | (0.2) | (0.2) | (1.7) | (1.7) |
| Site 7 | −16.1 | −40.5 | −5.6 | 38.2 | −24.1 | −17.6 | −6.4 |
| | (0.2) | (0.1) | (0.010) | (0.2) | (0.2) | (1.5) | (1.5) |

*See footnotes of Table 1; however, $\Delta G_{bind}$ was calculated according to Eq. 6.

## MM-PBSA for binding of myristate on HSA

We performed MM-PBSA calculations for the binding of MYR on HSA. Table 3 shows the calculated binding free energy components of HSA-1MYR complex based on the three-trajectory method. The binding free energy indicated large positive values at Sites 1, 3, 6, and 7, suggesting that these sites are low affinity binding sites for MYR. At Sites 2, 4, and 5, the binding free energy showed near-zero or negative values, indicating that they are high affinity MYR binding sites on HSA. The present MM-PBSA result was a little inconsistent with previous experimental work by Kragh-Hansen et al. (16), which reports that Sites 1, 5, and 4 are high affinity MYR binding sites on HSA. However, the group did not check the binding affinity of MYR at Site 2, because they have not yet produced mutants for Site 2 (16). Considering that only a small difference in carbon chain length exists between PLM (C16) and MYR (C14), similar binding modes are expected between these FAs. It might be

**TABLE 3 Binding free energy components of HSA-1MYR complex in the three-trajectory method (in units of kcal/mol)**

| | $\Delta E_{ele}$ | $\Delta E_{vdw}$ | $\Delta E_{int}$ | $\Delta G_{SA}$ | $\Delta G_{PB}$ | $\Delta G_{mmpbsa}$ | $T\Delta S$ | $\Delta G_{bind}$ |
|---|---|---|---|---|---|---|---|---|
| Site 1* | 225.9 | −26.4 | −1.5 | −4.2 | −172.0 | 21.8 | −16.2 | 38.0 |
| | (12.0) | (2.6) | (4.5) | (0.2) | (11.1) | (5.1) | (1.5) | (5.3) |
| Site 2 | 77.5 | −28.0 | 18.1 | −4.2 | −115.9 | −52.5 | −15.1 | −37.4 |
| | (11.8) | (2.6) | (4.6) | (0.1) | (10.3) | (5.5) | (3.1) | (6.3) |
| Site 3 | 339.6 | −40.6 | −6.6 | −3.4 | −268.3 | 20.7 | −19.7 | 40.4 |
| | (11.1) | (2.5) | (4.6) | (0.1) | (10.2) | (5.0) | (2.2) | (5.5) |
| Site 4 | 406.3 | −22.5 | −22.5 | −0.8 | −375.0 | −8.0 | −14.0 | 6.0 |
| | (11.1) | (2.4) | (4.5) | (0.1) | (10.4) | (5.0) | (1.9) | (5.3) |
| Site 5 | 440.6 | 13.9 | −11.7 | 1.6 | −458.7 | −14.2 | −21.4 | 7.2 |
| | (11.5) | (2.8) | (4.5) | (0.1) | (10.8) | (5.1) | (1.6) | (5.3) |
| Site 6 | 316.7 | −22.7 | −2.1 | −2.9 | −283.6 | 5.4 | −19.6 | 25.0 |
| | (12.0) | (2.6) | (4.5) | (0.1) | (11.0) | (5.0) | (2.0) | (5.4) |
| Site 7 | 204.0 | −1.0 | −2.3 | −3.2 | −194.0 | 8.1 | −21.5 | 29.7 |
| | (12.3) | (2.6) | (4.5) | (0.1) | (11.1) | (5.2) | (1.4) | (5.4) |

*See footnotes of Table 1.

possible that Site 2 and not Site 1 is one of the high affinity FA binding sites for MYR.

We also calculated binding free energy components of HSA-1MYR complex using the single-trajectory method (Table 4). Focusing on high affinity binding sites identified by the three-trajectory method (Sites 2, 4, and 5), the order of the binding free energy was $5 > 4 > 2$, thus corresponding to the present MM-PBSA calculations for PLM. Combining the results of the single-trajectory and three-trajectory methods, we identified Sites 2, 4, and 5 as high affinity MYR binding sites, where Site 5 was the highest affinity binding site, as is the case with PLM.

**TABLE 4 Binding free energy components of HSA-1MYR complex in the single-trajectory method (in units of kcal/mol)**

| | $\Delta E_{ele}$ | $\Delta E_{vdw}$ | $\Delta G_{SA}$ | $\Delta G_{PB}$ | $\Delta G_{mmpbsa}$ | $T\Delta S$ | $\Delta G_{bind}$ |
|---|---|---|---|---|---|---|---|
| Site 1* | −3.0 | −37.6 | −5.3 | 17.2 | −28.8 | −18.3 | −10.5 |
| | (0.1) | (0.2) | (0.01) | (0.2) | (0.2) | (1.0) | (1.0) |
| Site 2 | −7.9 | −39.2 | −5.5 | 27.0 | −25.5 | −22.0 | −3.6 |
| | (0.2) | (0.1) | (0.004) | (0.2) | (0.2) | (2.4) | (2.4) |
| Site 3 | −34.9 | −37.5 | −5.2 | 42.5 | −35.1 | −20.2 | −15.0 |
| | (0.3) | (0.2) | (0.01) | (0.2) | (0.2) | (1.4) | (1.4) |
| Site 4 | −6.4 | −36.9 | −5.3 | 18.3 | −30.3 | −18.7 | −11.7 |
| | (0.3) | (0.1) | (0.006) | (0.2) | (0.2) | (1.8) | (1.9) |
| Site 5 | −10.6 | −41.5 | −5.2 | 24.0 | −33.3 | −18.4 | −14.9 |
| | (0.2) | (0.1) | (0.006) | (0.2) | (0.2) | (1.1) | (1.1) |
| Site 6 | −4.2 | −39.4 | −5.2 | 21.8 | −27.0 | −21.4 | −5.6 |
| | (0.1) | (0.1) | (0.005) | (0.2) | (0.2) | (1.4) | (1.4) |
| Site 7 | −11.0 | −31.8 | −5.1 | 25.8 | −22.1 | −18.1 | −4.0 |
| | (0.4) | (0.1) | (0.007) | (0.4) | (0.2) | (2.2) | (2.2) |

*See footnotes of Table 1; however, $\Delta G_{bind}$ was calculated according to Eq. 6.

## Difference in ranking of the binding free energy between two types of MM-PBSA

The order of the magnitude of binding free energy at each FA binding site using the single-trajectory method did not coincide with that of the three-trajectory method, particularly for MYR. The difference between the two methods defines whether or not intramolecular strain, characterized as $\Delta E_{int}$, and induced fit effects are included with the calculated binding free energy. The intramolecular strain, caused by the binding of FA on HSA, was different at each FA binding site, as shown in Tables 1 and 3. Remarkable changes in strain were observed at Site 5 for PLM binding, and at Sites 2, 4, and 5 for MYR binding.

In addition, we analyzed how much induced fit occurred by the binding of FA to each FA binding site on HSA. Table 5 shows RMSDs of $C_\alpha$ atoms of unliganded HSA and HSA-1FA complex (5–8 ns) from unliganded HSA at 6 ns. RMSDs of each HSA-1FA complex binding site increased by FA binding, indicating that an induced fit effect occurred upon binding of FA to HSA. The extent of the increase in RMSD differed among FA binding sites, and more than 1 Å increase in RMSD was observed at Sites 1, 2, and 5 for PLM binding, and Sites 1 and 5 for MYR binding. It is interesting to note that the sites indicating large fluctuation (RMSD of $C_\alpha$ atoms) were not necessarily large in $\Delta E_{int}$, such as Site 1. By contraries, a large deviation was not observed at Site 3. If intramolecular strain was considered in the single-trajectory method (Table 4), the actual magnitude of the binding free energy of MYR might be larger at Sites 4 and 5 than at Site 3. This is because the intramolecular strain is more favorable at Sites 4 and 5, as shown in Table 3. In addition, taking into account the large conformational change observed at Site 5 by the binding of MYR, it is possible that the conformational change leads to more favorable FA—and thus highest—binding at Site 5. Although these differences do not directly explain the difference in the order of magnitude of binding free energy between the two methods, it is implied that both intramolecular strain and induced fit were intricately interrelated and caused a marked effect on the binding free energy.

**TABLE 5 Root mean-square deviation of each FA binding site of unliganded HSA and HSA-1FA complex (5–8 ns) from unliganded HSA at 6 ns (in units of Å)**

| | Palmitate | | Myristate | |
|---|---|---|---|---|
| | Unliganded | Complex | Unliganded | Complex |
| Site 1 (108–196) | 1.26 ± 0.32 | 2.62 ± 0.20 | 1.06 ± 0.16 | 2.10 ± 0.16 |
| Site 2 (1–297) | 1.75 ± 0.37 | 2.87 ± 0.18 | 1.38 ± 0.24 | 1.70 ± 0.22 |
| Site 3 (298–497) | 1.19 ± 0.16 | 2.07 ± 0.31 | 1.33 ± 0.21 | 1.69 ± 0.15 |
| Site 4 (384–497) | 0.91 ± 0.18 | 1.50 ± 0.10 | 1.02 ± 0.20 | 1.52 ± 0.10 |
| Site 5 (498–585) | 1.07 ± 0.22 | 2.08 ± 0.17 | 1.27 ± 0.27 | 3.41 ± 0.37 |
| Site 6 (197–383) | 1.19 ± 0.20 | 1.52 ± 0.15 | 1.30 ± 0.19 | 1.70 ± 0.16 |
| Site 7 (108–297) | 1.29 ± 0.30 | 2.00 ± 0.17 | 1.38 ± 0.29 | 1.97 ± 0.25 |

## Comparison of calculated binding free energy with experimental affinity data

How well do the binding free energies calculated by MM-PBSA calculations correspond to the experimental binding affinity constant? We compared the experimental affinity constants (27–29) with the calculated binding free energies of the single-trajectory method. Fig. 4 shows the relationship between experimental and calculated binding free energy for the three high affinity FA binding sites (Sites 2, 4, and 5). Many of the calculated binding free energies deviated greatly from the experimental binding free energies, as shown in Fig. 4. Furthermore, the calculated binding free energies of PLM were smaller than those of MYR. This result was inconsistent with previous reports showing that the magnitude of the affinity constant increased as the carbon chain length of the FA increased (16,27,29,50). It is reported that weak and strong binders that differ <2–3 orders of magnitude in $IC_{50}$ (corresponding to $\Delta\Delta G_{bind} \leq 4.8$ kcal/mol) are poorly distinguished by MM-PBSA (24), and this comparison between PLM and MYR may be attributed to this. More rigorous approaches are required to accurately estimate the binding free energy of each ligand.

On the other hand, the binding free energies calculated by the three-trajectory method (Tables 1 and 3) were much more deviated from the experimental binding free energies. As mentioned above, one of the reasons may be that the three-trajectory method is less precise than the single-trajectory method. Furthermore, the free energies ($G_{mmpbsa}$) of the two unliganded HSA models constructed from the HSA-7FA models were quite different between each other (−19,581.2 ± 93.7 kcal/mol and −17,633.2 ± 80.5 kcal/mol from HSA-7PLM complex and HSA-7MYR complex, respectively), suggesting that only a limited conformational space was used for the binding free energy calculation by the three-trajectory method. By sampling a full conformational space from each HSA and HSA-FA model, the calculated binding free energies may be more comparable with the experimental binding free energies; however, it is remarkably difficult to get enough conformational space of HSA, as in our previous study, reporting that even 10-ns MD simulations did not get a full impression of the conformational freedom of HSA (48).

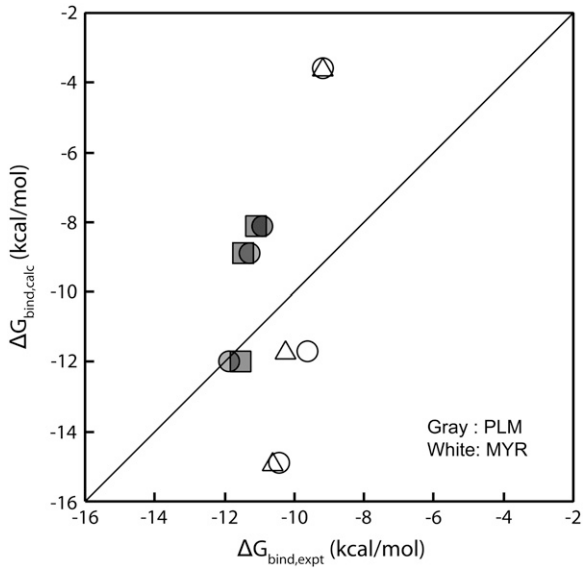


FIGURE 4 Relationship between experimental and calculated binding free energy for the three high affinity FA binding sites (Sites 5, 4, 2). Affinity constants ($K_1$, $K_2$, $K_3$) were taken from references, where the circle, triangle, and square symbols are corresponding to Ashbrook et al. (27), Pedersen et al. (28), and Richieri et al. (29). The experimental binding free energy ($\Delta G_{bind,expt}$) was calculated by $-RT \ln K$, where $R$ and $T$ are the gas constant and the absolute temperature, respectively.

## Change in radius of gyration of HSA by binding of fatty acids

Under normal physiological conditions, HSA binds with ~0.1–2 mol of FA per mol of protein (10), and the molar ratio of FA/HSA can rise up to 6 during fasting or maximum exercise (11,12). Based on these MD simulations, we analyzed conformational changes of unliganded HSA by the binding of FAs. Table 6 summarizes the radius of gyration ($Rg$) of unliganded HSA and HSA-1FA complexes, obtained from the 5- to 8-ns trajectory data from MD simulations. We modeled HSA under normal physiological conditions as the HSA-1FA complex in which FA is bound to Site 2, 4, or 5 (identified as high affinity FA binding sites), and during fasting or maximum exercise as the HSA-7FA complex. The binding of seven FA molecules to HSA caused an increase in $Rg$ of unliganded HSA, in line with previous studies (6,48). It is interesting that the binding of one FA molecule at Site 5 also caused a remarkable increase in $Rg$. In this study, Site 5 was identified as the highest binding affinity site, and it is suggested that induced fit caused the increase, as shown in Table 5. Thus, it is supposed that the total volume of HSA under normal physiological conditions is larger than that of unliganded HSA.

## CONCLUSION

In this study, high and low affinity FA binding sites on HSA were discussed quantitatively, based on the results of MM-PBSA calculations. According to the two trajectory set methods, three high affinity FA binding sites and the order of

**TABLE 6 Radius of gyration of unliganded HSA and HSA-FA complex based on 5- to 8-ns MD simulations (in units of Å)**

| | MYR | PLM |
|---|---|---|
| Unliganded HSA | 27.63 ± 0.10 | 27.61 ± 0.15 |
| HSA-7FA | 28.54 ± 0.17 | 28.40 ± 0.27 |
| HSA-1FA (Site 2) | 27.59 ± 0.11 | 27.81 ± 0.40 |
| HSA-1FA (Site 4) | 27.69 ± 0.12 | 27.67 ± 0.18 |
| HSA-1FA (Site 5) | 28.33 ± 0.15 | 27.90 ± 0.15 |

the magnitude of these three FA binding sites were identified for PLM and MYR. The radius of gyration of unliganded HSA increased remarkably by the binding of one FA molecule to the highest FA binding site, Site 5. Thus, this study revealed high and low FA binding sites for PLM and MYR, and possible conformational changes of HSA by the binding of FAs. In addition, this study illustrated the efficacy of combining the three-trajectory and single-trajectory methods. However, more rigorous approaches are required to accurately estimate the binding free energy. Nevertheless, the present MM-PBSA calculations agreed well with experimentally determined high and low FA binding sites. This analysis can be applied to the other FAs bound to HSA, as well as other ''one ligand bound to multiple binding sites'' systems. In conclusion, this study theoretically makes an important contribution to the identification of high affinity FA binding sites on HSA.

## SUPPLEMENTARY MATERIAL

To view all of the supplemental files associated with this article, visit www.biophysj.org.

This study was supported in part by Grants-in-Aid for Scientific Research from the Ministry of Education, Culture, Sports, Science, and Technology of Japan.

## REFERENCES

1. Kragh-Hansen, U., V. T. G. Chuang, and M. Otagiri. 2002. Practical aspects of the ligand-binding and enzymatic properties of human serum albumin. *Biol. Pharm. Bull.* 25:695–704.
2. He, X. M., and D. C. Carter. 1992. Atomic structure and chemistry of human serum albumin. *Nature.* 358:209–215.
3. Dockal, M., D. C. Carter, and F. Ruker. 1999. The three recombinant domains of human serum albumin. Structural characterization and ligand binding properties. *J. Biol. Chem.* 274:29303–29310.
4. Sugio, S., A. Kashima, S. Mochizuki, M. Noda, and K. Kobayashi. 1999. Crystal structure of human serum albumin at 2.5 Å resolution. *Protein Eng.* 12:439–446.
5. Ghuman, J., P. A. Zunszain, I. Petitpas, A. A. Bhattacharya, M. Otagiri, and S. Curry. 2005. Structural basis of the drug-binding specificity of human serum albumin. *J. Mol. Biol.* 353:38–52.
6. Curry, S., H. Mandelkow, P. Brick, and N. Franks. 1998. Crystal structure of human serum albumin complexed with fatty acid reveals an asymmetric distribution of binding sites. *Nat. Struct. Biol.* 5:827–835.
7. Curry, S., P. Brick, and N. Franks. 1999. Fatty acid binding to human serum albumin: new insights from crystallographic studies. *Biochim. Biophys. Acta.* 1441:131–140.
8. Bhattacharya, A. A., T. Grüne, and S. Curry. 2000. Crystallographic analysis reveals common modes of binding of medium and long-chain fatty acids to human serum albumin. *J. Mol. Biol.* 303:721–732.
9. Petitpas, I., T. Grüne, A. A. Bhattacharya, and S. Curry. 2001. Crystal structures of human serum albumin complexed with monounsaturated and polyunsaturated fatty acids. *J. Mol. Biol.* 314:955–960.
10. Fredrickson, D. S., and R. S. Gordon. 1958. The metabolism of albumin-bound $C^{14}$-labeled unesterified fatty acids in normal human subjects. *J. Clin. Invest.* 37:1504–1515.
11. Brodersen, R., S. Andersen, H. Volum, S. U. Nielsen, and A. O. Pedersen. 1990. Multiple fatty acid binding to albumin in human blood plasma. *Eur. J. Biochem.* 189:343–349.
12. Bahr, R., A. T. Høstmark, E. A. Newsholme, O. Grønnedød, and O. M. Sejersted. 1991. Effect of exercise on recovery changes in plasma levels of FFA, glycerol, glucose and catecholamines. *Acta Physiol. Scand.* 143:105–115.
13. Chuang, V. T., and M. Otagiri. 2002. How do fatty acids cause allosteric binding of drugs to human serum albumin? *Pharm. Res.* 19: 1458–1464.
14. Simard, J. R., P. A. Zunszain, C. E. Ha, J. S. Yang, N. V. Bhagavan, I. Petitpas, S. Curry, and J. A. Hamilton. 2005. Locating high-affinity fatty acid-binding sites on albumin by x-ray crystallography and NMR spectroscopy. *Proc. Natl. Acad. Sci. USA.* 102:17958–17963.
15. Simard, J. R., P. A. Zunszain, J. A. Hamilton, and S. Curry. 2006. Location of high and low affinity fatty acid binding sites on human serum albumin revealed by NMR drug-competition analysis. *J. Mol. Biol.* 361:336–351.
16. Kragh-Hansen, U., H. Watanabe, K. Nakajou, Y. Iwao, and M. Otagiri. 2006. Chain length-dependent binding of fatty acid anions to human serum albumin studied by site-directed mutagenesis. *J. Mol. Biol.* 363:702–712.
17. Rao, S. N., U. C. Singh, P. A. Bash, and P. A. Kollman. 1987. Free energy perturbation calculations on binding and catalysis after mutating Asn 155 in subtilisin. *Nature.* 328:551–554.
18. Hansson, T., J. Marelius, and J. Åqvist. 1998. Ligand binding affinity prediction by linear interaction energy methods. *J. Comput. Aided Mol. Des.* 12:27–35.
19. Srinivasan, J., T. E. Cheatham, P. Cieplak, P. A. Kollman, and D. A. Case. 1998. Continuum solvent studies of the stability of DNA, RNA, and phosphoramidate-DNA helices. *J. Am. Chem. Soc.* 120:9401–9409.
20. Wang, J., P. Morin, W. Wang, and P. A. Kollman. 2001. Use of MM-PBSA in reproducing the binding free energies to HIV-1 RT of TIBO derivatives and predicting the binding mode to HIV-1 RT of efavirenz by docking and MM-PBSA. *J. Am. Chem. Soc.* 123:5221–5230.
21. Huo, S., J. Wang, P. Cieplak, P. A. Kollman, and I. D. Kuntz. 2002. Molecular dynamics and free energy analyses of cathepsin D-inhibitor interactions: insight into structure-based ligand design. *J. Med. Chem.* 45:1412–1419.
22. Fogolari, F., A. Brigo, and H. Molinari. 2003. Protocol for MM/PBSA molecular dynamics simulations of proteins. *Biophys. J.* 85:159–166.
23. Gohlke, H., and D. A. Case. 2004. Converging free energy estimates: MM-PB(GB)SA studies on the protein-protein complex Ras-Raf. *J. Comput. Chem.* 25:238–250.
24. Kuhn, B., P. Gerber, T. Schulz-Gasch, and M. Stahl. 2005. Validation and use of the MM-PBSA approach for drug discovery. *J. Med. Chem.* 48:4040–4048.
25. Xu, Y., and R. Wang. 2006. A computational analysis of the binding affinities of FKBP12 inhibitors using the MM-PB/SA method. *Proteins.* 64:1058–1068.
26. Saifer, A., and L. Goldman. 1961. The free fatty acids bound to human serum albumin. *J. Lipid Res.* 2:268–270.
27. Ashbrook, J. D., A. A. Spector, E. C. Santos, and J. E. Fletcher. 1975. Long chain fatty acid binding to human plasma albumin. *J. Biol. Chem.* 250:2333–2338.
28. Pedersen, A. O., and R. Brodersen. 1988. Myristic acid binding to human serum albumin investigated by dialytic exchange rate. *J. Biol. Chem.* 263:10236–10239.
29. Richieri, G. V., A. Anel, and A. M. Kleinfeld. 1993. Interactions of long-chain fatty acids and albumin: determination of free fatty acid levels using the fluorescent probe ADIFAB. *Biochemistry.* 32:7574–7580.
30. Berman, H. M., J. Westbrook, Z. Feng, G. Gilliland, T. N. Bhat, H. Weissig, I. N. Shindyalov, and P. E. Bourne. 2000. The Protein Data Bank. *Nucleic Acids Res.* 28:235–242.
31. Case, D. A., T. A. Darden, T. E. Cheatham, III, C. L. Simmerling, J. Wang, R. E. Duke, R. Luo, K. M. Merz, B. Wang, D. A. Pearlman,

M. Crowley, S. Brozell, V. Tsui, H. Gohlke, J. Mongan, V. Hornak, G. Cui, P. Beroza, C. Schafmeister, J. W. Caldwell, W. S. Ross, and P. A. Kollman. AMBER8. University of California, San Francisco, CA.

32. Cornell, W. D., P. Cieplak, C. I. Bayly, I. R. Gould, K. M. Merz Jr., D. M. Ferguson, D. C. Spellmeyer, T. Fox, J. W. Caldwell, and P. A. Kollman. 1995. A second generation force field for the simulation of proteins, nucleic acids, and organic molecules. *J. Am. Chem. Soc.* 117: 5179–5197.
33. Wang, J., R. M. Wolf, J. W. Caldwell, P. A. Kollman, and D. A. Case. 2004. Development and testing of a general Amber force field. *J. Comput. Chem.* 25:1157–1173.
34. Frisch, M. J., G. W. Trucks, H. B. Schlegel, G. E. Scuseria, M. A. Robb, J. R. Checseman, J. A. Montgomery Jr, T. Vrcven, K. N. Kudin, J. C. Burant, J. C. Millam, S. S. Iyengar, J. Tomasi, V. Barone, B. Mennucci, M. Cossi, G. Scalmani, N. Rega, G. A. Petersson, H. Nakatsuji, M. Hada, M. Ehara, K. Toyota, R. Fukuda, J. Hasegawa, M. Ishida, T. Nakajima, Y. Honda, O. Kitao, H. Nakai, M. Klene, X. Li, J. E. Knox, H. P. Hratchian, J. B. Cross, C. Adamo, J. Jaramillo, R. Gomperts, R. E. Stratmann, O. Yazyev, A. J. Austin, R. Cammi, C. Pomelli, J. W. Ochterski, P. Y. Ayala, K. Morokuma, G. A. Voth, P. Salvador, J. J. Dannenberg, V. G. Zakrzewski, S. Dapprich, A. D. Daniels, M. C. Strain, O. Farkas, D. K. Malick, A. D. Rabuck, K. Raghavachari, J. B. Foresman, J. V. Ortiz, Q. Cui, A. G. Baboul, S. Clifford, J. Cioslowski, B. B. Stefanov, G. Liu, A. Liashenko, P. Piskorz, I. Komaromi, R. L. Martin, D. J. Fox, T. Keith, M. A. Al-Laham, C. Y. Peng, A. Nanayakkara, M. Challacombe, P. M. W. Gill, B. Johnson, W. Chen, M. W. Wong, C. Gonzalez, and J. A. Pople. GAUSSIAN 03, Revision A.1. Gaussian, Pittsburgh, PA.
35. Bayly, C. I., P. Cieplak, W. D. Cornell, and P. A. Kollman. 1993. A well-behaved electrostatic potential based method using charge restraints for deriving atomic charges. The RESP model. *J. Phys. Chem.* 97:10269–10280.
36. Accelrys, Inc. DISCOVERY STUDIO. Accelrys, San Diego, CA.
37. Jorgensen, W. L., J. Chandrasekhar, J. D. Madura, R. W. Impey, and M. L. Klein. 1983. Comparison of simple potential functions for simulating liquid water. *J. Chem. Phys.* 79:926–935.
38. Darden, T., D. York, and L. Pedersen. 1993. Particle mesh Ewald—an Nlog(N) method for Ewald sums in large systems. *J. Chem. Phys.* 98: 10089–10092.
39. Van Gunsteren, W. F., and H. J. C. Berendsen. 1977. Algorithm for macromolecular dynamics and constraint dynamics. *Mol. Phys.* 34: 1311–1327.
40. Berendsen, H. J. C., J. P. M. Postma, W. F. van Gunsteren, A. DiNola, and J. R. Haak. 1984. Molecular dynamics with coupling to an external bath. *J. Chem. Phys.* 81:3684–3690.
41. Honig, B., and A. Nicholls. 1995. Classical electrostatics in biology and chemistry. *Science.* 268:1144–1149.
42. Sitkoff, D., K. A. Sharp, and B. Honig. 1994. Accurate calculation of hydration free-energies using microscopic solvent models. *J. Phys. Chem.* 98:1978–1988.
43. McQuarrie, D. A. 1976. Statistical Mechanics. Harper & Row, NY.
44. Kottalam, J., and D. A. Case. 1990. Langevin modes of macromolecules: application to crambin and DNA hexamers. *Biopolymers.* 29:1409–1421.
45. Lanig, H., O. G. Othersen, F. R. Beierlein, U. Seidel, and T. Clark. 2006. Molecular dynamics simulations of the tetracycline-repressor protein: the mechanism of induction. *J. Mol. Biol.* 359:1125–1136.
46. Celik, L., J. D. D. Lund, and B. Schiøtt. 2007. Conformational dynamics of the estrogen receptor $\alpha$: molecular dynamics simulations of the influence of binding site structure on protein dynamics. *Biochemistry.* 46:1743–1758.
47. Zoete, V., M. Meuwly, and M. Karplus. 2005. Study of the insulin dimerization: binding free energy calculations and per-residue free energy decomposition. *Proteins.* 61:79–93.
48. Fujiwara, S., and T. Amisaki. 2006. Molecular dynamics study of conformational changes in human serum albumin by binding of fatty acids. *Proteins.* 64:730–739.
49. Masukawa, K. M., P. A. Kollman, and I. D. Kuntz. 2003. Investigation of neuraminidase-substrate recognition using molecular dynamics and free energy calculations. *J. Med. Chem.* 46:5628–5637.
50. Pedersen, A. O., B. Honoré, and R. Brodersen. 1990. Thermodynamic parameters for binding of fatty acids to human serum albumin. *Eur. J. Biochem.* 190:497–502.
51. Humphrey, W., A. Dalke, and K. Schulten. 1996. VMD—visual molecular dynamics. *J. Mol. Graph.* 14:33–38.